


Eigenenergies and quantum transport properties in a non-Hermitian quantum-dot chain with side-coupled dots

Lian-Lian Zhang, Ze-Zhong Li, Guo-Hui Zhan, Guang-Yu Yi, and Wei-Jiang Gong*
College of Sciences, Northeastern University, Shenyang 110819, China

 (Received 26 January 2018; revised manuscript received 18 October 2018; published 22 March 2019)

We study the eigenenergies of a one-dimensional quantum-dot chain with its each dot side coupling to two additional dots. It is found that when the \mathcal{PT} -symmetric complex potentials are introduced to the side-coupled dots, the eigenlevel degeneracy is broken. However, further increasing the complex potentials induces a kind of two-degree degeneracy of the eigenlevels. This is accompanied by the \mathcal{PT} -symmetry breaking, with the appearance of the complex part of the eigenlevels. These changes exactly affect the quantum transport properties of the chain. First, in the case of weak \mathcal{PT} -symmetric complex potentials, a group of transmission function peaks arise at the center of the transmission function spectrum. When the eigenlevel degeneracy takes place, the degenerated eigenlevels decouple from the leads and the corresponding peaks disappear in the transmission function spectra. We believe that this work provides helpful information for a better understanding of the eigenenergies and quantum transport properties in non-Hermitian systems.

DOI: [10.1103/PhysRevA.99.032119](https://doi.org/10.1103/PhysRevA.99.032119)

I. INTRODUCTION

In the past decades, parity-time (\mathcal{PT}) symmetry has been studied in many fields, such as optics [1–6], matter waves [7,8], electronics [9,10], acoustics [11], and magnonics [12]. The theoretical basis of this research progress originates from the fact that \mathcal{PT} -symmetric non-Hermitian Hamiltonians can exhibit real eigenenergy spectra [13,14]. It has also been demonstrated that one important feature of \mathcal{PT} -symmetric Hamiltonians is the existence of spontaneous symmetry breaking, which has been observed in many photonic structures, including directional couplers [15], switching devices [16,17], plasmonic structure [18], and topological insulators [19]. Accordingly, the special properties of the \mathcal{PT} -symmetric systems have attracted considerable attention from both theoretical and experimental aspects [20–22]. Recently, Chitsazi *et al.* fabricated the Floquet \mathcal{PT} -symmetric system that consists of two ultrahigh frequency oscillators coupled by a time-dependent capacitance. They found that a cascade of \mathcal{PT} -symmetric broken domains are bounded by exceptional point degeneracies [23].

The experimental developments motivate more researchers to explore the \mathcal{PT} -symmetric systems of non-Hermitian Hamiltonians. And then, the physics properties of these systems have become one important concern in this field [20,24–27]. Recently, Rivolta *et al.* investigated the topological features of a one-dimensional photonic quasicrystal within the context of \mathcal{PT} symmetry, especially the presence of interface modes in the band gaps [28]. It has been found that the mix of order and disorder of this system gives a useful basis for exploring how the \mathcal{PT} -symmetry-related effects are interrelated. Besides, some other groups have dedicated themselves to the research about the \mathcal{PT} -symmetric

systems of non-Hermitian Hamiltonians, and some interesting phenomena have been reported [29–33], e.g., the special band structure and quantum states. One of the attractive conclusions is that the \mathcal{PT} -symmetric complex potentials play nontrivial roles in modulating the quantum interference that governs the quantum transport process [34,35]. For instance, in a non-Hermitian triple-quantum-dot structure, the \mathcal{PT} -symmetric complex potentials are able to induce the shift of antiresonance, changes from antiresonance to resonance, and occurrence of new antiresonance [36].

In view of the above results, one can ascertain that the \mathcal{PT} -symmetric non-Hermitian systems indeed exhibit interesting properties, whereas more discussions should be performed, for further understanding these systems. In the present work, we would like to pay attention to one \mathcal{PT} -symmetric non-Hermitian system and study the effect of \mathcal{PT} -symmetric complex potentials on its eigenenergies and transport properties. This system is composed of a one-dimensional quantum-dot (QD) chain with each QD connecting with two additional QDs laterally. It shows that when the \mathcal{PT} -symmetric complex potentials are introduced to the side-coupled QDs, the degeneracy of the eigenlevels is broken. Instead, a kind of two-degree eigenlevel degeneracy comes into being with the further increase of these potentials. At the same time, one can find the breaking of the \mathcal{PT} symmetry, with the appearance of the complex part of the eigenlevels. Next, we can readily find that such changes influence the quantum transport properties of the chain. In the case of weak \mathcal{PT} -symmetric complex potentials, a group of the transmission function spectrum arises. When the eigenlevel degeneracy takes place, the degenerated eigenlevels decouple from the leads, and then the corresponding peaks disappear in the transmission function spectra.

II. THEORETICAL MODEL

The QD chain that we consider is shown in Fig. 1, in which each QD couples to two QDs additionally which are

*gwj@mail.neu.edu.cn

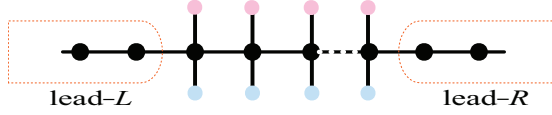


FIG. 1. Schematic of a non-Hermitian QD chain, whose terminal QDs of the chain couple to lead-L and lead-R, respectively. In addition, each QD in the chain couples to two QDs laterally, which are affected by the \mathcal{PT} -symmetric complex on-site chemical potentials.

affected by the \mathcal{PT} -symmetric complex potentials. In order to investigate its transport properties, the terminal QDs are assumed to connect with two leads, i.e., lead-L and lead-R, respectively. The Hamiltonian of this system can be written as

$$H = H_L + H_R + H_d + H_T, \quad (1)$$

with its each part given by

$$H_L = \sum_{n=-1}^{\infty} t_0 c_n^\dagger c_{n-1} + \text{H.c.},$$

$$H_R = \sum_{n=1}^{\infty} t_0 c_n^\dagger c_{n+1} + \text{H.c.},$$

$$H_d = \sum_{l=1}^N \varepsilon_l d_l^\dagger d_l + \left(\sum_{l=1}^{N-1} t_l d_{l+1}^\dagger d_l + \text{H.c.} \right) + \sum_{l=1}^N \sum_{j=1}^2 \xi_{lj} b_{lj}^\dagger b_{lj} + \left(\sum_{l=1}^N \sum_{j=1}^2 v_{lj} b_{lj}^\dagger d_l + \text{H.c.} \right),$$

$$H_T = t_L c_{-1}^\dagger d_1 + t_R c_1^\dagger d_N + \text{H.c.} \quad (2)$$

c_n^\dagger (c_n) is to create (annihilate) a fermion at the n th site of the two semi-infinite leads with t_0 being the hopping amplitude between the nearest sites. d_l^\dagger (d_l) is the creation (annihilation) operator for QD- l of the QD chain with energy level ε_l , and t_l denotes the interdot coupling between QD- $(l+1)$ and QD- l . b_{lj}^\dagger (b_{lj}) is the operator to create (annihilate) a fermion at the j th QD that couples to QD- l in the QD chain with energy level ξ_{lj} , and v_{lj} represents the interdot coupling. Next, $t_{L(R)}$ is the tunneling amplitude between the terminal QDs in the QD main and lead-L(R).

In order to study the quantum transport through this structure, the transmission function in this system should be calculated. According to the previous works, the calculation can be performed via a variety of methods [37,38]. In this work, we would like to choose the transfer-matrix method to study the transport properties of this system, by deriving the analytical formula of the transmission coefficient.

To begin with, we would like to write out the wave function of the system as $|\psi\rangle = \sum_n c_n(\tau)|\phi_n\rangle + \sum_l (d_l(\tau)|d_l\rangle + \sum_j b_{lj}(\tau)|b_{lj}\rangle)$ with $|\phi_n\rangle = c_n^\dagger|0\rangle$, $|d_l\rangle = d_l^\dagger|0\rangle$, and $|b_{lj}\rangle = b_{lj}^\dagger|0\rangle$. By substituting expression of $|\psi\rangle$ into the Schrödinger equation $i\partial\tau|\psi\rangle = H|\psi\rangle$, the following coupled-mode equations can be obtained for the expansion coefficients c_n and d_l :

$$i\dot{c}_n = t_0 c_{n-1}(1 - \delta_{n,1}) + t_0 c_{n+1}(1 - \delta_{n,N}) + t_L d_1 \delta_{n,-1} + t_R d_N \delta_{n,1}, \quad (3)$$

$$i\dot{d}_l = \varepsilon_l d_l + t_l^* d_{l+1}(1 - \delta_{l,N}) + t_{l-1} d_{l-1}(1 - \delta_{l,1}) + \sum_{j=1}^2 v_{lj} b_{lj} + t_L^* c_{-1} \delta_{l,1} + t_R^* c_1 \delta_{l,N}, \quad (4)$$

$$i\dot{b}_{lj} = \xi_{lj} b_{lj} + v_{lj} d_l, \quad (5)$$

where t_0 has been assumed to be real. The stationary solution can be expressed in the following form: $c_n(\tau) = A_n e^{-i\omega\tau}$, $d_l(\tau) = B_l e^{-i\omega\tau}$, and $b_{lj}(\tau) = C_{lj} e^{-i\omega\tau}$. And then, we can obtain the algebraic relationship of the amplitudes on each site:

$$\omega A_n = t_0 A_{n-1}(1 - \delta_{n,1}) + t_0 A_{n+1}(1 - \delta_{n,N}) + t_L B_1 \delta_{n,-1} + t_R B_N \delta_{n,1}, \quad (6)$$

$$\omega B_l = \varepsilon_l B_l + t_l^* B_{l+1}(1 - \delta_{l,N}) + t_{l-1} B_{l-1}(1 - \delta_{l,1}) + \sum_{j=1}^2 v_{lj}^* C_{lj} + t_L^* A_{-1} \delta_{l,1} + t_R^* A_1 \delta_{l,N}, \quad (7)$$

$$\omega C_{lj} = \xi_{lj} C_{lj} + v_{lj} B_l. \quad (8)$$

Substituting Eq. (8) into Eq. (7), one can write out an equation that includes A_n and B_l , i.e.,

$$(\omega - \tilde{\varepsilon}_l) B_l = t_l^* B_{l+1}(1 - \delta_{l,N}) + t_{l-1} B_{l-1}(1 - \delta_{l,1}) + t_L^* A_{-1} \delta_{l,1} + t_R^* A_1 \delta_{l,N}, \quad (9)$$

where $\tilde{\varepsilon}_l = \varepsilon_l + \sum_j \frac{|v_{lj}|^2}{\omega - \xi_{lj}}$. With the help of Eq. (6) and Eq. (9), one can get the matrix equation that

$$\mathcal{D} \begin{bmatrix} B_1 \\ B_2 \\ \vdots \\ B_{N-1} \\ B_N \end{bmatrix} = \begin{bmatrix} t_L^* A_{-1} \\ 0 \\ \vdots \\ 0 \\ t_R^* A_1 \end{bmatrix}, \quad (10)$$

in which \mathcal{D} is a tridiagonal matrix, defined as

$$\mathcal{D} = \begin{bmatrix} \omega - \tilde{\varepsilon}_1 & -t_1^* & 0 & \cdots & 0 \\ -t_1 & \omega - \tilde{\varepsilon}_2 & -t_2^* & \cdots & 0 \\ \vdots & & \ddots & & \vdots \\ 0 & & & \omega - \tilde{\varepsilon}_{N-1} & -t_{N-1}^* \\ 0 & & \cdots & -t_{N-1} & \omega - \tilde{\varepsilon}_N \end{bmatrix}. \quad (11)$$

After solving the tridiagonal matrix (See Appendix A), we can express B_1 and B_N in terms of A_{-1} and A_1 :

$$B_1 = \frac{1}{\det \mathcal{D}} [\mathcal{D}_{11} t_L^* A_{-1} + (-1)^{N+1} \mathcal{D}_{N1} t_R^* A_1],$$

$$B_N = \frac{1}{\det \mathcal{D}} [(-1)^{N+1} \mathcal{D}_{1N} t_L^* A_{-1} + \mathcal{D}_{NN} t_R^* A_1],$$

in which \mathcal{D}_{ji} is the algebraic cofactor of determinant $\det \mathcal{D}$. This allows us to construct the equations that relate to A_{-1} and A_1 , i.e.,

$$\begin{aligned} (\omega - \mu_{-1,-1}) A_{-1} &= t_0 A_{-2} + \mu_{-1,1} A_1, \\ (\omega - \mu_{1,1}) A_1 &= t_0 A_2 + \mu_{1,-1} A_{-1}, \end{aligned} \quad (12)$$

with

$$\begin{aligned}\mu_{-1,-1} &= \frac{\mathcal{D}_{11}}{\det \mathcal{D}} |t_L|^2, \\ \mu_{-1,1} &= (-1)^{N+1} \frac{\mathcal{D}_{N1}}{\det \mathcal{D}} t_L t_R^*, \\ \mu_{1,-1} &= (-1)^{N+1} \frac{\mathcal{D}_{1N}}{\det \mathcal{D}} t_L^* t_R, \\ \mu_{1,1} &= \frac{\mathcal{D}_{NN}}{\det \mathcal{D}} |t_R|^2.\end{aligned}$$

Such two equations are important to describe the scattering properties in this system.

Next, we evaluate the scattering properties in this system. To do so, it is necessary for us to write out the trial wave

$$\tau = \frac{t_0 \mu_{1,-1} (e^{ik} - e^{-ik})}{(\omega - \mu_{-1,-1})(\omega - \mu_{1,1}) - \mu_{1,-1} \mu_{-1,1} - t_0 e^{ik} (2\omega - \mu_{-1,-1} - \mu_{1,1}) + t_0^2 e^{2ik}}. \quad (14)$$

Surely, the transmission function (TF), defined as $T(\omega) = |\tau|^2$, can be discussed with the help of the transmission-amplitude expression.

In discrete systems, \mathcal{P} and \mathcal{T} are defined as the space-reflection (parity) operator and the time-reversal operator. If a Hamiltonian obeys the commutation relation $[\mathcal{PT}, H] = 0$, it will be said to be \mathcal{PT} symmetric. In our considered structure, the effect of the \mathcal{P} operator is to let $\mathcal{P}d_{N+1-i}\mathcal{P} = d_i$ and $\mathcal{P}b_{l1}\mathcal{P} = b_{l2}$, and the effect of the \mathcal{T} operator is $\mathcal{T}i\mathcal{T} = -i$. Thus, it is not difficult to find that the Hamiltonian is invariant under the combined operation \mathcal{PT} , under the condition of $t_l = t_c$, $v_{lj} = v_c$, $\varepsilon_l = \varepsilon_{N+1-l}^*$, and $\xi_{l1} = \xi_{l2}^*$ for uniform QD-lead couplings. In this work, we would like to add the \mathcal{PT} -symmetric complex potentials to the two side-coupled QDs to investigate their effects on the quantum transport process. Thus, we take $\varepsilon_l = \varepsilon_0$ and $\xi_{l1(l2)} = \xi \pm i\gamma$ to perform discussion. In practice, $\pm i\gamma$ represent the physical gain or loss during the interacting processes between the environment and the side-coupled QDs.

III. NUMERICAL RESULTS AND DISCUSSIONS

In the following, we would like to first investigate the eigenenergies of the one-dimensional QD chain and then focus on its quantum transport properties by introducing two leads to couple to the chain. For the structural parameters, we take $\varepsilon_l = \xi_{lj} = 0$ and $v_c = t_c = 0.5$, respectively. Surely, the QD in the chain and its side-coupled QDs can be viewed as one cell. And then, we are allowed to view the QD chain as one N -cell geometry.

A. Eigenenergies of the \mathcal{PT} -symmetric non-Hermitian QD chain

It is known that in the absence of \mathcal{PT} -symmetric complex potentials, the QD chain is Hermitian, and its eigenenergies can be analytically solved, i.e., $e_j = t_c \cos k \pm \sqrt{t_c^2 \cos^2 k + 2v_c^2}$ with $k = \frac{j}{N+1}\pi$ ($j = 1 \rightarrow N$), whereas the

function as

$$A_n = \begin{cases} e^{ikn} + r e^{-ikn} & (n < 0), \\ \tau e^{ikn} & (n > 0). \end{cases}$$

By substituting the expression of A_n into Eq. (12), we can get the equations that include r and τ , i.e.,

$$\begin{aligned} & \begin{bmatrix} (\omega - \mu_{-1,-1})e^{ik} - t_0 e^{2ik} & -\mu_{-1,1} e^{ik} \\ -\mu_{1,-1} e^{ik} & (\omega - \mu_{1,1})e^{ik} - t_0 e^{2ik} \end{bmatrix} \\ & \begin{bmatrix} r \\ \tau \end{bmatrix} = \begin{bmatrix} -(\omega - \mu_{-1,-1})e^{ik} + t_0 e^{-2ik} \\ \mu_{1,-1} e^{-ik} \end{bmatrix}. \end{aligned} \quad (13)$$

Via a straightforward deduction, the analytical form of the transmission amplitude can be expressed, i.e.,

other N eigenlevels degenerate at the energy zero point. When \mathcal{PT} -symmetric complex potentials are applied, the eigenenergies are certain to be modified. In order to present a detailed analysis, we would like to discuss the eigenenergies by increasing the cell number from one. In the case of $\varepsilon_0 = \xi = 0$, the three eigenenergies of the $N = 1$ chain can be analytically written out, i.e., $\tilde{e}_1 = -\sqrt{2v_c^2 - \gamma^2}$, $\tilde{e}_2 = 0$, and $\tilde{e}_3 = \sqrt{2v_c^2 - \gamma^2}$, respectively. One can readily find that the \mathcal{PT} -symmetric complex potentials indeed modulate the eigenenergies in a substantial way. As γ increases to its critical point $\gamma = \sqrt{2}v_c$, \tilde{e}_1 and \tilde{e}_3 will degenerate, equal to \tilde{e}_2 as well. This point is the so-called exceptional point (EP). Next when γ further increases, \tilde{e}_1 and \tilde{e}_3 will become imaginary, leading to the occurrence of \mathcal{PT} -symmetry breaking. The numerical results are shown in Figs. 2(a) and 2(b), from which the variation of the eigenenergies can be well clarified.

We then increase the number of the cells in the quantum chain to observe the changes of its eigenenergies. The relevant calculation can refer to Appendix A, and the results of N from 2 to 5 are shown in Fig. 3. Figures 3(a) and 3(b) show the real and imaginary parts of the eigenenergies of the $N = 2$ structure. One can find that in the case of $\gamma = 0$, there are five

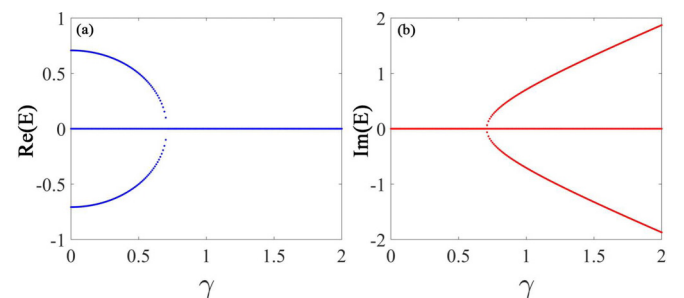


FIG. 2. Spectra of the eigenenergies of the \mathcal{PT} -symmetric chain with $N = 1$, affected by the presence of \mathcal{PT} -symmetric complex potentials. Relevant parameters are taken to be $\varepsilon_l = \xi_{lj} = 0$ and $v_c = 0.5$. (a) and (b) Description of the real and imaginary parts of the eigenenergies.

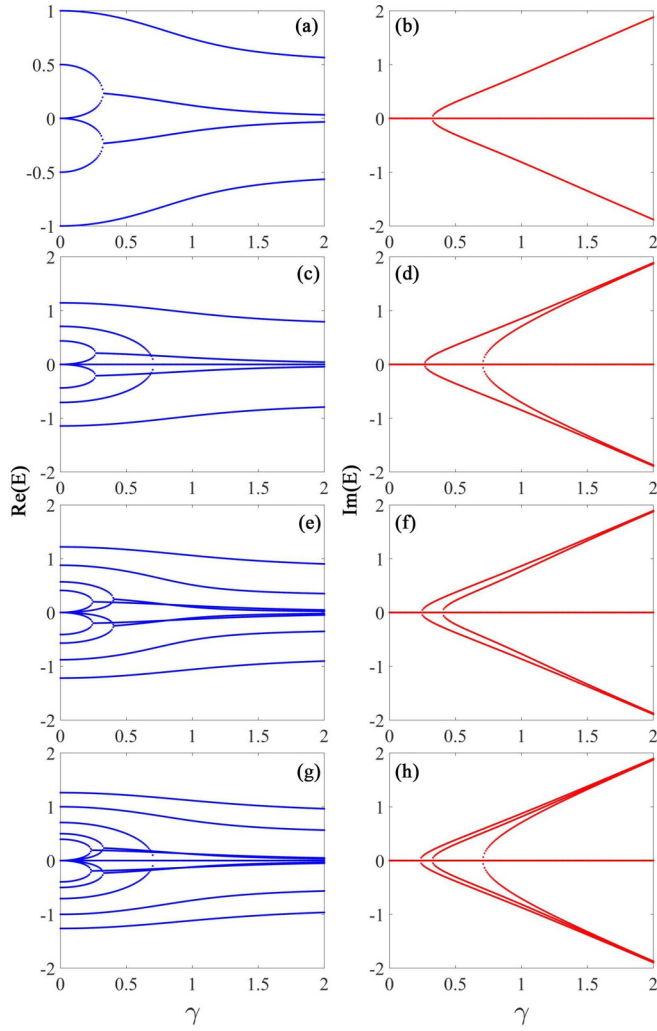


FIG. 3. Real and imaginary parts of the eigenenergies of the QD chain with its cell number from 2 to 5, affected by the presence of \mathcal{PT} -symmetric complex potentials. Relevant parameters are taken to be $\varepsilon_l = \xi_{lj} = 0$ and $t_c = v_c = 0.5$. (a) and (b) Real and imaginary parts of $N = 2$; (c) and (d) results of $N = 3$; (e) and (f) $N = 4$; (g) and (h) $N = 5$.

eigenenergies of double-cell chain, i.e., $\tilde{e}_1 = -\tilde{e}_5 = -1.0$, $\tilde{e}_2 = -\tilde{e}_4 = 0.5$, and $\tilde{e}_3 = 0$. Once the nonzero γ is taken into account, e_3 splits into two, i.e., $\tilde{e}_3^{(1)}$ and $\tilde{e}_3^{(2)}$. And the values of these two levels increase with the increment of γ . In this process, however, the magnitudes of the other levels decrease. At the EP of $\gamma \approx 0.27$, level degeneracy takes place between \tilde{e}_2 and $\tilde{e}_3^{(1)}$, as well as \tilde{e}_4 and $\tilde{e}_3^{(2)}$. Thus, in this geometry, the \mathcal{PT} -symmetric complex potentials first induce the breaking of the level degeneracy at the energy zero point and then lead to the occurrence of new level degeneracy [see Fig. 3(a)]. In addition, it shows that when the new degeneracy occurs, the imaginary part of the eigenenergies begins to come into being. This exactly indicates that the \mathcal{PT} symmetry of the quantum chain is spontaneously broken in this situation.

As for the triple-cell structure, from Figs. 3(c) and 3(d) we see that similar to the double-cell case, one small γ can induce the level splitting around the energy zero point, i.e., from \tilde{e}_4 to $\tilde{e}_4^{(j)}$ ($j = 1 \rightarrow 3$). Also, the increase of γ to $\gamma = 0.2$ gives rise to the occurrence of level degeneracy of \tilde{e}_3 and $\tilde{e}_4^{(1)}$ (and \tilde{e}_5 and $\tilde{e}_4^{(3)}$). Note that since the QD number is odd, the eigenlevel at the energy zero point is robust with the increase of γ . Next when γ increases to 0.7, the other level degeneracy takes place, with $\tilde{e}_2 = \tilde{e}_6 = 0$ in this case. This level degeneracy is accompanied by the appearance of the imaginary part of the chain's eigenenergies, as shown in Fig. 3(d). The eigenenergies of the structure of $N = 4$ and 5 are exhibited in Figs. 3(e)–3(h), respectively. By comparing these results with those of $N = 2$ and 3, we can conclude that the influence of γ on the eigenenergies of the quantum chain is tightly dependent on the parity of N . To be specific, for the N -cell structure ($N \in \text{even}$), there will occur N pairs of level degeneracy with the increase of γ . In this process, the two levels \tilde{e}_N and $\tilde{e}_{N+1}^{(1)}$ first show degeneracy, then \tilde{e}_{N-1} and $\tilde{e}_{N+1}^{(2)}$ degenerate, and so on. And then, $\frac{N}{2}$ EPs appear. For the case of odd cells, the other two levels $\tilde{e}_{\frac{1}{2}(N+1)}$ and $\tilde{e}_{\frac{3}{2}(N+1)}$ can also degenerate with the further increase of γ . As a consequence, $\frac{N+1}{2}$ EPs exist and N eigenlevels do not degenerate at last. When the level degeneracy takes place, the new imaginary part of the eigenenergies comes into play at the same time. It is certain that the level degeneracy of the real part of the eigenenergies is one signature of the breaking of the \mathcal{PT} symmetry of this QD chain.

In Fig. 4, we take the triple-cell and four-cell structures to present the eigenenergy variation behaviors, by supposing the \mathcal{PT} -symmetric potentials to act on the partial side-coupled QDs. We here would like to concentrate on two cases, i.e., these potentials acting on the ending and nonending cells, respectively. To be concrete, Figs. 4(a)–4(d) describe the results of the triple-cell structure, and the four-cell results are shown in Figs. 4(e)–4(h), respectively. It can be found that similar to those in Fig. 3, the existence of γ can lead to the eigenlevel degeneracy, and the imaginary part of the eigenenergies appear at the same time. However, the original degeneracy at the energy zero point cannot be destroyed by the complex potentials in these cases. As shown in Fig. 4(a), the eigenlevel degeneracy takes place between the levels \tilde{e}_3 and \tilde{e}_7 in the former case of the triple-cell structure. In its latter case, two extra levels, i.e., e'_2 and e'_8 , emerge simultaneously with the increase of γ . Next, they get closer to each other and degenerate in the situation of $\gamma = 0.7$. With respect to the four-cell structure, it can be found in Figs. 4(e)–4(f) that in the former case, the two pairs of eigenlevels that are symmetric about the energy zero point, i.e., \tilde{e}_4 and \tilde{e}_9 (\tilde{e}_3 and \tilde{e}_{10}), degenerate when γ increases to 0.6. Instead, in the latter case, when the \mathcal{PT} -symmetric potentials are introduced, the degeneracy at the energy zero point is broken partially. One then finds the degeneracy between \tilde{e}_4 and $\tilde{e}_5^{(1)}$ in Fig. 4(g), similar to that in Fig. 3(e). Therefore, when \mathcal{PT} -symmetric complex potentials are introduced to the sid-coupled QD partially, the eigenlevel degeneracy and the imaginary part of the eigenenergies occur in an alternative manner.

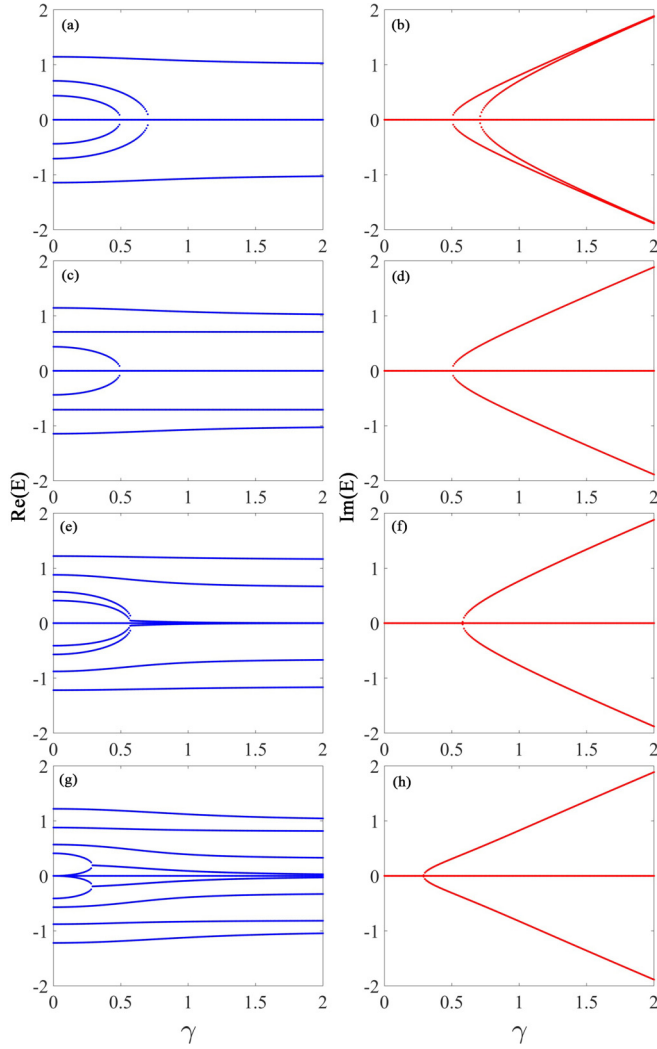


FIG. 4. Real and imaginary parts of the eigenenergies of the $N = 3$ and $N = 4$ chains due to \mathcal{PT} -symmetric complex potentials applied on the side-coupled QDs partially. (a)–(d) Results of $N = 3$ structure when the potentials applied on the ending and nonending cells. (e)–(h) Corresponding results of the structure of $N = 4$.

The above result arouses us to pay attention to the influence of the \mathcal{PT} -symmetric complex potentials on the band structure of one infinitely long QD chain with side-coupled QDs. In the presence of \mathcal{PT} -symmetric complex potentials, the band structure of the infinitely long QD chain obeys the equation that

$$E^3 - \omega_0 E^2 + (\gamma^2 - 2v_c^2)E - \omega_0 \gamma^2 = 0, \quad (15)$$

with $\omega_0 = 2t_c \cos k$. According to the result in Appendix B, E_1 is always real, and it changes continuously with the increase of γ [see Fig. 5(a)]. On the other hand, E_2 and E_3 have an opportunity to become complex in this process. As a result, they are mutually conjugate with each other, as shown in Figs. 5(b) and 5(c). This reflects the spontaneous breaking of the \mathcal{PT} symmetry of this system. In Fig. 5(c), it shows that increasing γ indeed gives rise to the appearance of the imaginary part of E_2 , with the clear critical position of EP. Then, Eq. (B3) allows us to write out the critical

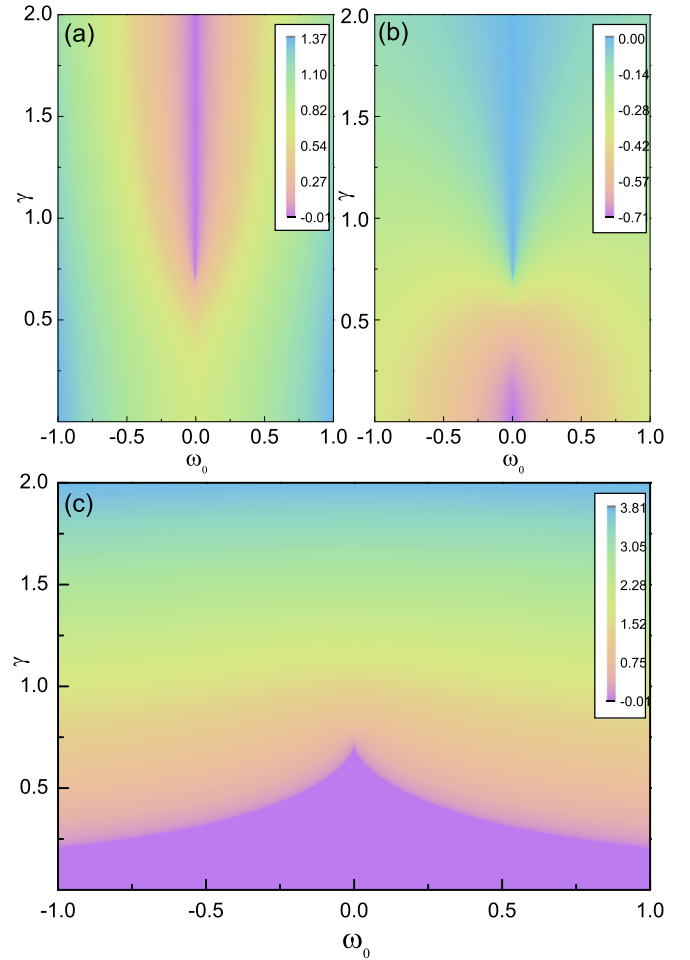


FIG. 5. (a) Spectrum of the real eigenenergy (i.e., E_1) of the infinitely long QD chain. (b) and (c) Real and imaginary parts of E_2 .

condition, i.e.,

$$6v_c^2 - 3\gamma^2 + \omega_0^2 = [9\omega_0(v_c^2 + \gamma^2) + \omega_0^3]^{2/3}. \quad (16)$$

This further helps us to clarify the influences of \mathcal{PT} -symmetric complex potentials on the eigenenergies of our considered QD chain.

B. Quantum transport properties of the \mathcal{PT} -symmetric QD chain

In this subsection, we introduce two leads to couple to the ending cells and evaluate the influence of the \mathcal{PT} -symmetric complex potentials on the quantum transport properties in the QD chain. The TF obeys the relationship of $T(\omega) = |\tau|^2$ with τ expressed in Eq. (14). Prior to calculation, we take $t_0 = 1.0$. The structural parameters of the QD chain are the same as in the above subsection, respectively.

Without loss of generality, we first choose the triple-cell structure as an example to present the influence of the \mathcal{PT} -symmetric potentials on the quantum transport behaviors. The numerical results are shown in Fig. 6. In Fig. 6(a), it can be found that in the absence of \mathcal{PT} -symmetric potentials, six resonant peaks appear in the TF spectrum, distributing

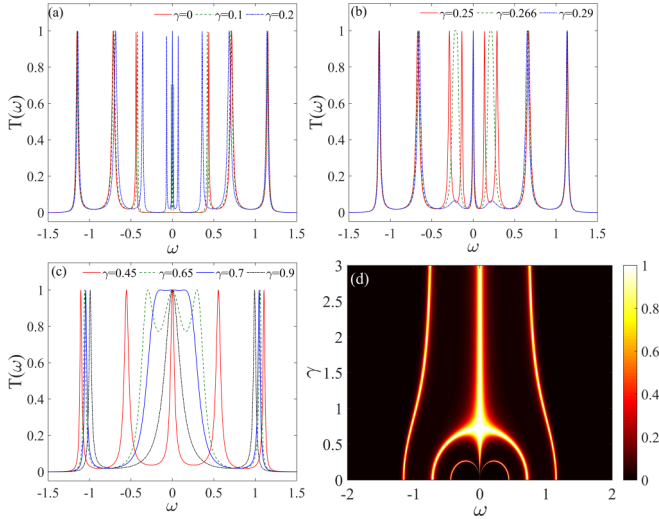


FIG. 6. Spectra of the TF of the triple-cell system, following the increase of \mathcal{PT} -symmetric complex potentials. The chain-lead coupling is taken to be $t_\alpha = 0.1$.

at the points of $\omega = \frac{\sqrt{2}}{4}(\pm 1 \pm \sqrt{5})$ and $\pm \frac{\sqrt{2}}{2}$, respectively, which are completely consistent with the eigenenergies of the chain. When the complex potentials are applied, three new peaks emerge around the energy zero point. And increasing the potentials can widen the three peaks, with the enlargement of their distance, as shown by the line of $\gamma = 0.25$ in Fig. 6(b). Meanwhile, the peaks at the points of $\omega = \pm \frac{\sqrt{2}}{4}(\sqrt{5} - 1)$ shift to the energy zero point. This change exactly originates from the shift of the eigenenergies of the QD chain [see Fig. 3(c)]. Next, one can observe that with the increase of γ , the peaks beside the energy zero point merge to one and then are suppressed, until their disappearance. As a result, only five peaks survive in the TF spectrum. Thus we know that the level degeneracy induces the decoupling mechanism, which leads to the disappearance of the corresponding TF peaks. If the complex potentials are further increased, the two peaks beside the energy zero point get closer and merge to one, corresponding to the second level degeneracy. This further verifies the relationship between the level degeneracy and decoupling. The more visual change of the TF peaks can be observed in Fig. 6(d). Accordingly, we can understand the role of the \mathcal{PT} -symmetric potentials in modifying the TF spectrum.

Next, in Figs. 7(a)–7(c) we plot the TF spectra of the structure of $N = 2, 3$, and 5, by considering the presence of \mathcal{PT} -symmetric potentials. It is evident that the relation between the TF peaks and the eigenenergies is well defined, as shown in Figs. 7(a)–7(c). Taking the TF spectrum of $N = 2$ as an example, four TF peaks appear at the points of $\omega = \pm 0.5$ and ± 1.0 in the case of $\gamma = 0$. In the presence of the complex potentials, two new peaks generate near the energy zero point, and their distance is proportional to the value of γ . Following the increase of γ , the peaks at the points of $\omega = \pm 0.5$ get closer to the two split peaks, respectively, until the occurrence of the level degeneracy. Similar to those in Fig. 6, when the level degeneracy takes place, the corresponding peaks will disappear. Such a phenomenon can also be observed in

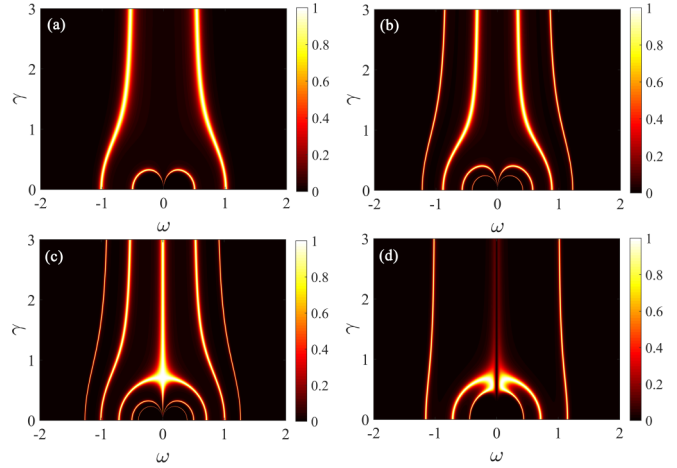


FIG. 7. (a)–(c) TF spectra of the systems of $N = 2, 3$, and 5, due to the increase of \mathcal{PT} -symmetric complex potentials. The chain-lead coupling is taken to be $t_\alpha = 0.1$. (d) Results of the triple-cell structure when the complex potentials are applied on the ending cells.

Figs. 7(b) and 7(c). And then, the influence of \mathcal{PT} -symmetric complex potentials can be further clarified. Note, also, that when N is odd, the TF peak at the energy zero point is robust for the case of nonzero γ . However, in Fig. 7(d) it shows that when the complex potentials are applied on the partial cells, an alternative result will come into being. Here for the triple-cell structure with the complex potentials on the ending cells, no TF peak appears at the energy zero point, despite the occurrence of level degeneracy.

We next consider the case of strong QD-lead coupling to calculate the TF, i.e., $T(\omega)$. The left column of Fig. 8 shows the TF spectra for the structures with $N = 1$ –4. From this figure we can see that in the case of $N = 1$, one antiresonance point (i.e., the zero value of the TF) occurs at the position of $\omega = 0$. Such a result is easy to understand based on the expression of $\tilde{\epsilon}_l$, i.e., $\tilde{\epsilon}_l = \epsilon_l + \frac{2v_c^2}{\omega - \xi}$. In the case of $\omega = \xi$, $\tilde{\epsilon}_l$ will be equal to infinity, which inevitably eliminates the quantum transport in this system. According to the previous works, this antiresonance point arises from the destructive interference induced by the side-coupled QDs [39,40]. It is evident that the two peaks coincide with the first and third eigenstates of the triple QDs, respectively. When N increases from 1 to 3, one can find that both edges of the antiresonance valley become steep rapidly. As a result, one well-defined insulating band forms around the antiresonance point in the region of $-0.4 < \omega < 0.4$. This means that in such a QD chain with side-coupled QDs, the antiresonance valley changes into a well-defined insulating band when $N \geq 3$. Accordingly, the TF spectrum is divided into two groups with an insulating band in between. With the expression of the band structure, i.e., $E_k = t_c \cos k \pm \sqrt{t_c^2 \cos^2 k + 2v_c^2}$, we can obtain the gap between the two groups as $\Delta E_g = 2(\sqrt{t_c^2 + 2v_c^2} - t_c)$. One can clearly find that the insulating band in the TF spectrum is well consistent with the value of ΔE_g . However, note that such a result arises from the antiresonance effect in the quantum transport process, as explained in our previous works [40]. Since each cell induces the antiresonance phenomenon, we can know that the serially coupling of identical cells inevitably

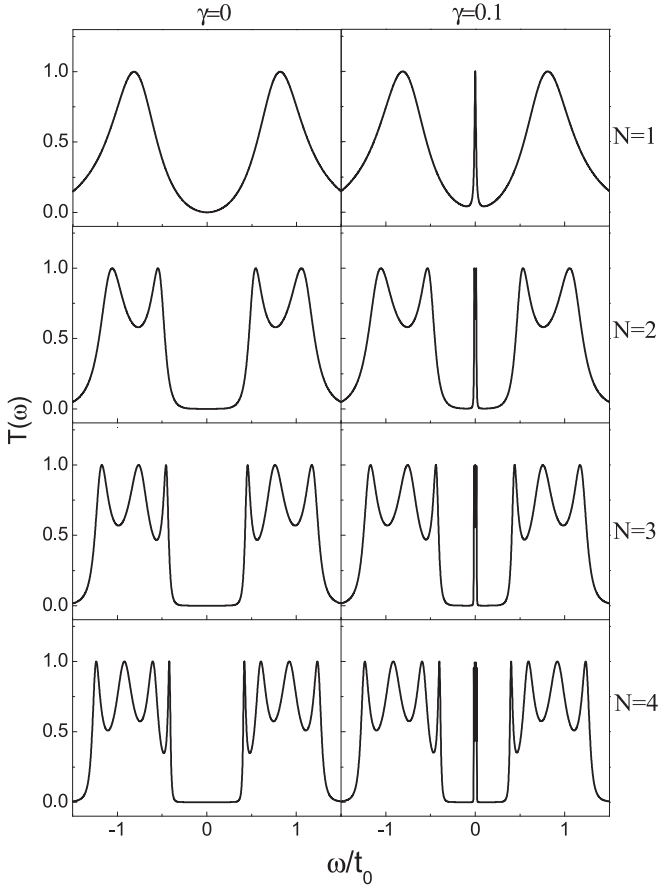


FIG. 8. Spectra of the TF of our considered system, in the absence and presence of \mathcal{PT} -symmetric complex potentials. Relevant parameters are taken to be $\varepsilon_l = \xi_{lj} = 0$ and $t_c = v_c = t_\alpha = 0.5$.

enhances the destructive quantum interference around the antiresonance point, leading to the early appearance of the insulating band. Next, we introduce the \mathcal{PT} -symmetric complex potentials to the side-coupled QDs, to investigate the change of the insulating band in the TF spectra. The numerical results are shown in the right column of Fig. 7, where the magnitude of the potentials is supposed to be $\gamma = 0.1$. It shows that for the structure of $N = 1$, the antiresonance at the energy zero point is replaced by one resonant peak, as the \mathcal{PT} -symmetric potentials are taken into account. Next, with the lengthening of the QD chain, resonant peaks can also appear at the energy zero point, however, the insulating band in the TF spectrum still survives.

As the \mathcal{PT} -symmetric complex potentials are enhanced, the resonant peak in the insulating band will undergo a clear change, as shown in Fig. 9. In this figure, we take the cases of $N = 3$ and $N = 4$ to present the influence of increasing γ . It can be found that if $N = 3$ with $\gamma = 0.2$, the three resonant peaks in the insulating band are widened obviously. This certainly destroys the insulating band in the TF spectrum. Meanwhile, the two peaks beside the insulating band are also widened, so the band edges become less sharp. All these changes cause the TF spectrum to exhibit a simple three-group structure in this case. Next, if the magnitude of the

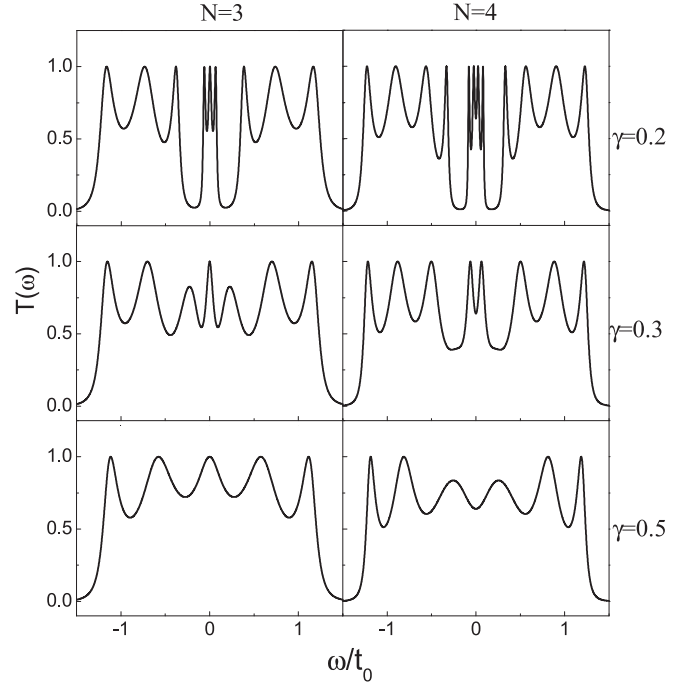


FIG. 9. TF spectra of the $N = 3$ and $N = 4$ systems, influenced by the increase of \mathcal{PT} -symmetric complex potentials. The other parameters are the same as those in Fig. 2.

\mathcal{PT} -symmetric potentials increases to $\gamma = 0.3$, the mark of the insulating band will disappear completely, with the three-group structure of the TF spectrum alike. Furthermore, when $\gamma = 0.5$, the TF spectrum exactly exhibits the single-group result with five peaks. A similar process can be observed in the right column of Fig. 9 where $N = 4$. Therefore, even by a little increase of \mathcal{PT} -symmetric complex potentials, the insulating band in the TF spectrum can be destroyed seriously.

In order to further understand the effect of the \mathcal{PT} -symmetric complex potentials, we take the cases of $N = 3$ and $N = 4$ to investigate the TF spectrum when such potentials act on the side-coupled QDs partially. First, we consider the case of $N = 3$ where these potentials act on the side-coupled QDs of the ending cells, with the results shown in Fig. 10(a). One can find that in such a case, the increase of γ suppresses the peaks beside the insulating band, leading to the smoothness of the insulating-band edges. However, no peak appears in the insulating band. Next, in Fig. 10(b), the \mathcal{PT} -symmetric potentials are applied on the nonending cell. It can be seen that the weak complex potentials can only narrow the insulating band, whereas the shape of the insulating band almost holds. Accordingly, the insulating band can be eliminated with the increase of γ . We can clearly find that when γ increases to 0.5, one resonant peak appears at the energy zero point. This result can be explained by analyzing the expression of $T(\omega)$. In such a case, $g_1^{-1} = \omega - \frac{2v_c^2}{w} - \Sigma_L$ and $g_3^{-1} = \omega - \frac{2v_c^2}{w} - \Sigma_R$ where $\Sigma_\alpha = |t_\alpha|^2 g_0$ and $g_\alpha = g_0 = \frac{\omega}{2t_0^2} - \frac{\rho_0}{2}i$ with $\rho_0 = \sqrt{4t_0^2 - \omega^2}/t_0^2$ [41,42]. Consequently, at the low-energy

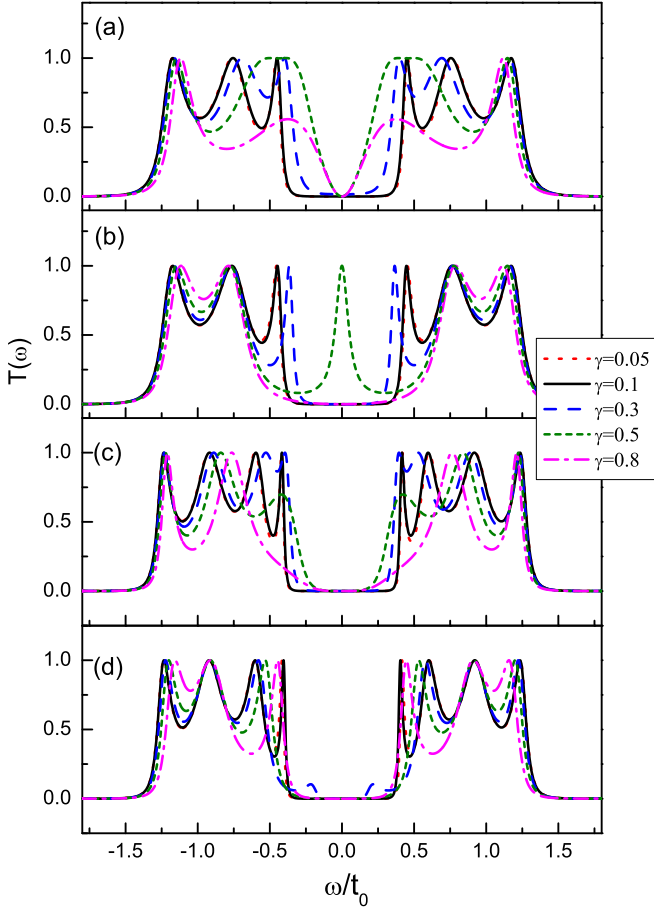


FIG. 10. Spectra of the TF of our considered system, influenced by the increase of \mathcal{PT} -symmetric complex potentials. (a) and (b) $N = 3$ results of the potentials applied on the ending and nonending cells, respectively. (c) and (d) Corresponding results of the $N = 4$ structure.

limit it can be simplified as

$$T(\omega)|_{N=3} = \frac{\omega^2 \Gamma^L \Gamma^R t_c^4}{[4v_c^2 [v_c^2 \frac{\gamma^2 - 2v_c^2}{\gamma^2} + t_c^2] + (\Sigma_L + \Sigma_R)\omega [2v_c^2 \frac{\gamma^2 - 2v_c^2}{\gamma^2} + t_c^2]]^2},$$

in which $\Gamma^\alpha = i(\Sigma_\alpha - \Sigma_\alpha^\dagger)$. It is not difficult to find that in the critical case of $t_c = v_c = \gamma$, $T(\omega = 0)|_{N=3} = \frac{\Gamma^L \Gamma^R}{|\Sigma_L + \Sigma_R|^2}$, which will be equal to 1.0 for the symmetric QD-lead coupling. However, when γ further increases, e.g., $\gamma = 0.8$, the insulating band comes into being at the energy zero point again. However, its edges become rather smooth. Next for the chain of $N = 4$, it shows in Figs. 10(c) and 10(d) that in the former case, the TF peaks decrease and the antiresonance valley becomes apparently widened, with the increase of γ . Instead, in the latter case, the insulating band is stable when the \mathcal{PT} -symmetric potentials are presented, regardless of the decrease of the TF peaks.

IV. SUMMARY

To sum up, in this work we have investigated the eigenenergies and transport properties of a one-dimensional QD chain

with each QD side coupling to two additional QDs. It has been found that when the \mathcal{PT} -symmetric complex potentials are introduced to the side-coupled QDs, the eigenlevel degeneracy at the energy zero point is broken. However, further increasing the complex potentials induces a kind of two-degree degeneracy of the eigenlevels, with the appearance of the complex part of the eigenlevels. This exactly corresponds to the breaking of the \mathcal{PT} symmetry. It shows that when the cell number of the QD chain N is even, $\frac{N}{2}$ EPs can be observed, whereas $\frac{N+1}{2}$ EPs exist for the odd N . As a consequence, these degeneracy changes modify the quantum transport properties of the chain. On the one hand, in the case of weak \mathcal{PT} -symmetric complex potentials, a group of TF peaks arises at the center of the TF spectrum. On the other hand, when the additional eigenlevel degeneracy takes place, the degenerated eigenlevels decouple from the leads and the corresponding peaks disappear in the TF spectra. In addition, for the strong chain-lead coupling, the insulating band in the TF spectrum can be efficiently destroyed by the complex potentials. All the results have been analyzed in detail. It can be certain that this work is helpful for understanding the \mathcal{PT} symmetry and the corresponding quantum transport properties in non-Hermitian systems.

ACKNOWLEDGMENT

Our work was financially supported by the Fundamental Research Funds for the Central Universities (Grant No. N180503020).

APPENDIX A: PROPERTY OF TRIDIAGONAL MATRIX

Here we give an analytical treatment of the determinant of a $N \times N$ tridiagonal matrix, which is written as

$$\mathcal{D} = \begin{bmatrix} \varepsilon_1 & t_1^* & 0 & \cdots & 0 \\ t_1 & \varepsilon_2 & t_2^* & \cdots & 0 \\ \vdots & & \ddots & & \vdots \\ 0 & & & \varepsilon_{N-1} & t_{N-1}^* \\ 0 & \cdots & t_{N-1} & & \varepsilon_N \end{bmatrix}. \quad (\text{A1})$$

By using a relation as $\det \mathcal{D}_j = \varepsilon_j \det \mathcal{D}_{j+1} - |t_j|^2 \det \mathcal{D}_{j+2}$, where $\det \mathcal{D}_j$ is a submatrix of \mathcal{D} , we can obtain an analytical expression about the determinant $\det \mathcal{D}$. After a straightforward deduction, we can write it in terms of a product of the inversed continued fractions,

$$\det \mathcal{D} = \frac{\det \mathcal{D}}{\det \mathcal{D}_2} \frac{\det \mathcal{D}_2}{\det \mathcal{D}_3} \cdots \frac{\det \mathcal{D}_{N-1}}{\det \mathcal{D}_N} \det \mathcal{D}_N = [X_1 X_2 \cdots X_{N-1}]^{-1} \varepsilon_N, \quad (\text{A2})$$

where the continued fraction X_j is defined as

$$X_j = \frac{1}{\varepsilon_j - \frac{|t_j|^2}{\varepsilon_{j+1} - \frac{|t_{j+1}|^2}{\varepsilon_{j+2} - \cdots - \frac{|t_{N-2}|^2}{\varepsilon_{N-1} - \frac{|t_{N-1}|^2}{\varepsilon_N}}}}}. \quad (\text{A3})$$

Surely, as a special case where $\varepsilon_j = \varepsilon_0$ and $t_j = t_c$, the eigenvalues of such a tridiagonal matrix take a simple analytical

form, i.e.,

$$e_m = \varepsilon_0 + 2|t_c|^2 \cos \frac{m\pi}{N+1}. \quad (\text{A4})$$

APPENDIX B: SOLUTION OF THE CUBIC EQUATION

For Eq. (15), one can obtain its solutions with the help of the mathematical knowledge. To be concrete, its real solution is given by

$$E_1 = \frac{1}{3}\omega_0 - \frac{\sqrt[3]{2}A}{3\sqrt[3]{B + \sqrt{4A^3 + B^2}}} + \frac{1}{3\sqrt[3]{2}}\sqrt[3]{B + \sqrt{4A^3 + B^2}}, \quad (\text{B1})$$

and the complex solutions are

$$E_2 = E_3^* = \frac{1}{3}\omega_0 + \frac{(1 + i\sqrt{3})A}{3\sqrt[3]{4\sqrt[3]{B + \sqrt{4A^3 + B^2}}}} - \frac{(1 - i\sqrt{3})}{6\sqrt[3]{2}}\sqrt[3]{B + \sqrt{4A^3 + B^2}}, \quad (\text{B2})$$

with A and B defined as $A = -6v_c^2 + 3\gamma^2 - \omega_0^2$ and $B = 18\omega_0(v_c^2 + \gamma^2) + 2\omega_0^3$, respectively. Based on the expression of $E_{2(3)}$, we can get the critical condition that its nonzero imaginary part begins to appear. Via a straightforward deduction, one can find that in such a case, there will be

$$A = -\left(\frac{B}{2}\right)^{\frac{2}{3}}. \quad (\text{B3})$$

-
- [1] K. G. Makris, R. El-Ganainy, D. N. Christodoulides, and Z. H. Musslimani, *Phys. Rev. Lett.* **100**, 103904 (2008).
- [2] S. Longhi, *Phys. Rev. Lett.* **103**, 123601 (2009).
- [3] A. Regensburger, C. Bersch, M. A. Miri, G. Onishchukov, D. N. Christodoulides, and U. Peschel, *Nature (London)* **488**, 167 (2012).
- [4] N. Lazarides and G. P. Tsironis, *Phys. Rev. Lett.* **110**, 053901 (2013).
- [5] D. Wang and A. B. Aceves, *Phys. Rev. A* **88**, 043831 (2013).
- [6] L. Feng, Z. L. Wong, R. M. Ma, Y. Wang, and X. Zhang, *Science* **346**, 972 (2014).
- [7] H. Cartarius and G. Wunner, *Phys. Rev. A* **86**, 013612 (2012).
- [8] W. D. Heiss, H. Cartarius, and G. Wunner, *J. Phys. A* **46**, 275307 (2013).
- [9] H. Ramezani, J. Schindler, F. M. Ellis, U. Günther, and T. Kottos, *Phys. Rev. A* **85**, 062122 (2012).
- [10] N. Bender, S. Factor, J. D. Bodyfelt, H. Ramezani, D. N. Christodoulides, F. M. Ellis, and T. Kottos, *Phys. Rev. Lett.* **110**, 234101 (2013).
- [11] X. Zhu, H. Ramezani, C. Shi, J. Zhu, and X. Zhang, *Phys. Rev. X* **4**, 031042 (2014).
- [12] A. Galda and V. M. Vinokur, *Phys. Rev. B* **94**, 020408(R) (2016).
- [13] C. M. Bender and S. Boettcher, *Phys. Rev. Lett.* **80**, 5243 (1998).
- [14] C. M. Bender, *Rep. Prog. Phys.* **70**, 947 (2007).
- [15] H. Benisty, A. Lupu, and A. Degiron, *Phys. Rev. A* **91**, 053825 (2015).
- [16] S. Phang, A. Vukovic, H. Susanto, T. M. Benson, and P. Sewell, *J. Opt. Soc. Am. B* **30**, 2984 (2013).
- [17] N. X. A. Rivolta and B. Maes, *J. Opt. Soc. Am. B* **32**, 1330 (2015).
- [18] H. Benisty, A. Degiron, A. Lupu, A. D. Lustrac, S. Chénais, S. Forget, M. Besbes, G. Barbillon, A. Bruyant, S. Blaize, and G. Lérondel, *Opt. Exp.* **19**, 18004 (2011).
- [19] M. Z. Hasan and C. L. Kane, *Rev. Mod. Phys.* **82**, 3045 (2010).
- [20] A. Guo, G. J. Salamo, D. Duchesne, R. Morandotti, M. Volatier-Ravat, V. Aimez, G. A. Siviloglou, and D. N. Christodoulides, *Phys. Rev. Lett.* **103**, 093902 (2009).
- [21] Z. P. Liu, J. Zhang, S. K. Özdemir, B. Peng, H. Jing, X. Y. Lü, C. W. Li, L. Yang, F. Nori, and Y. X. Liu, *Phys. Rev. Lett.* **117**, 110802 (2016).
- [22] B. Peng, S. K. Ozdemir, S. Rotter, H. Yilmaz, M. Liertzer, F. Monifi, C. M. Bender, F. Nori, and L. Yang, *Science* **346**, 328 (2014).
- [23] M. Chitsazi, H. Li, F. M. Ellis, and T. Kottos, *Phys. Rev. Lett.* **119**, 093901 (2017).
- [24] M. Znojil, *Phys. Rev. A* **82**, 052113 (2010).
- [25] J. Schindler, A. Li, M. C. Zheng, F. M. Ellis, and T. Kottos, *Phys. Rev. A* **84**, 040101(R) (2011).
- [26] C. E. Rüter, K. G. Makris, R. El-Ganainy, D. N. Christodoulides, M. Segev, and D. Kip, *Nat. Phys.* **6**, 192 (2010).
- [27] A. Regensburger, M. A. Miri, C. Bersch, J. Näger, G. Onishchukov, D. N. Christodoulides, and U. Peschel, *Phys. Rev. Lett.* **110**, 223902 (2013).
- [28] N. X. A. Rivolta, H. Benisty, and B. Maes, *Phys. Rev. A* **96**, 023864 (2017).
- [29] B. G. Zhu, R. Lü, and S. Chen, *Phys. Rev. A* **89**, 062102 (2014).
- [30] O. Bendix, R. Fleischmann, T. Kottos, and B. Shapiro, *Phys. Rev. Lett.* **103**, 030402 (2009).
- [31] L. Jin and Z. Song, *Phys. Rev. A* **80**, 052107 (2009); W. H. Hu, L. Jin, Y. Li, and Z. Song, *ibid.* **86**, 042110 (2012).
- [32] Y. N. Joglekar and A. Saxena, *Phys. Rev. A* **83**, 050101(R) (2011).
- [33] G. D. Valle and S. Longhi, *Phys. Rev. A* **87**, 022119 (2013).
- [34] L. Jin and Z. Song, *Phys. Rev. A* **85**, 012111 (2012).
- [35] B. Zhu, Rong Lü, and S. Chen, *Phys. Rev. A* **91**, 042131 (2015).
- [36] L. L. Zhang and W. J. Gong, *Phys. Rev. A* **95**, 062123 (2017).
- [37] S. Datta, *Electron Transport in Mesoscopic Systems* (Cambridge University Press, Cambridge, 1997).
- [38] Y. Meir and N. S. Wingreen, *Phys. Rev. Lett.* **68**, 2512 (1992);

- A. P. Jauho, N. S. Wingreen, and Y. Meir, *Phys. Rev. B* **50**, 5528 (1994).
- [39] X. R. Wang, Yupeng Wang, and Z. Z. Sun, *Phys. Rev. B* **65**, 193402 (2002).
- [40] W. Gong, Y. Zheng, Y. Liu, and T. Lü, *Phys. Rev. B* **73**, 245329 (2006).
- [41] W. J. Gong, X. Y. Sui, Y. Wang, G. D. Yu, and X. H. Chen, *Nanoscale Research Lett.* **8**, 330 (2013); W. J. Gong, S. F. Zhang, Z. C. Li, G. Yi, and Y. S. Zheng, *Phys. Rev. B* **89**, 245413 (2014).
- [42] S. Zhang, W. Gong, G. Wei, and A. Du, *J. Appl. Phys.* **109**, 023704 (2011).